



Cooperative learning formation control of multiple autonomous underwater vehicles with prescribed performance based on position estimation

Zilong Song^a, Zheyuan Wu^a, Haocai Huang^{a,b,c,d,*}

^a Ocean College, Zhejiang University, Zhoushan, 316021, China

^b Laboratory for Marine Geology, Qingdao National Laboratory for Marine Science and Technology, Qingdao, 266061, China

^c Hainan Institute of Zhejiang University, Hainan, 572025, China

^d Donghai Laboratory, Zhoushan, 316021, China

ARTICLE INFO

Handling Editor: Prof. A.I. Incecik

Keywords:

Autonomous underwater vehicles

Multi-agent systems

Finite-time control

Distributed observer

Deterministic learning

ABSTRACT

This paper proposes a cooperative learning formation control method with finite-time prescribed performance based on position estimation for parametric path tracking of multiple autonomous underwater vehicles (AUVs) with uncertainties and external disturbances. The parametric path used in the control law permits the velocity to be specified independently while tracking the path accurately. The localized radial basis function neural networks learn the uncertainties cooperatively while tracking the period path, and the knowledge gained from learning is utilized to construct an empirically based formation control law using experience to cope with similar uncertainties rather than repeatedly using adaptive methods, which reduces the computing burden. The position of the leader is assumed to be available only for the leader's neighboring AUV, and a novel finite-time distributed observer is presented for the followers to estimate the leader's position. Based on this, the control law is derived from the prescribed performance control method using a finite-time performance function rather than exponential decaying function to enable the tracking error converges in finite time, which accelerates the learning process. The simulation results confirm the validity of the presented control protocol.

1. Introduction

Autonomous underwater vehicles (AUVs) have received a significant amount of attention in recent years owing to their outstanding advantages in applications such as pipeline detection, military defense, and ocean observation (Peng et al., 2019; Qiao and Zhang, 2020; Rong et al., 2022; Shen et al., 2018; Zhou et al., 2022; Zong et al., 2021). With the increasing complexity of underwater missions, multiple AUVs working in a collaborative fashion often have advantages over individual AUV operations, which has motivated the research on the formation control of AUVs. In recent years, many excellent works on formation problem of AUVs have been presented (Liu et al., 2021a; Peng et al., 2020; Xu et al., 2022a, 2022b).

The complexity of multi-AUV formation control comes from several aspects, including complex model nonlinear dynamics and time-varying external disturbances in the environment. Existing studies have proposed some effective approaches to address the above problems. RBFNN

is extensively utilized to approximate unknown dynamics (Cui et al., 2017b; Fang et al., 2021; Wu and Huang, 2022; Zong et al., 2021), and the coping strategies for external disturbances include disturbance observer (Gao and Guo, 2020; Lin et al., 2021; Liu et al., 2017; Lv et al., 2022), extended state observer (Cui et al., 2017a; Kong et al., 2021; Wei et al., 2021), etc.

The above literature has fully investigated the use of various strategies to control AUVs to accurately track the reference path, however, these methods did not take into account control of the velocity during path tracking. In addition, existing studies (Cui et al., 2017b; Fang et al., 2021; Wu and Huang, 2022; Zong et al., 2021) have utilized the global approximation capability of RBFNN while neglecting the local learning capability and cooperative capability of RBFNN.

The localized RBFNN employed in (Dai et al., 2022; Wang and Wang, 2015) is capable of learning the uncertainties when tracking the periodic path with the error converging asymptotically. However, the deterministic learning imposes a demand on the convergence rate of the

* Corresponding author. Institute of Ocean Engineering and Technology, Ocean College, Zhejiang University, Zhoushan, 316021, China.

E-mail addresses: zilong.song@zju.edu.cn (Z. Song), wuzheyuan@zju.edu.cn (Z. Wu), hchuang@zju.edu.cn (H. Huang).

system, since learning can initiate only after the system has converged, as evidenced by (Wang and Hill, 2006). Prescribed performance control was implemented in (Bechlioulis et al., 2017; Huang et al., 2021; Liu et al., 2021b) in which the error was limited by the performance function to achieve better dynamic performance. Furthermore, the finite-time performance function utilized in (Fu and Wang, 2021; Sun et al., 2021) is enabled to specify the convergence time in advance.

The above discussion is based on the assumption that agents have access to the states of all other agents, which is impractical in AUV formation control due to hardware limitations, transmission failure, energy costs, and other factors. Specifically, the position of the leader is available only for the leader's neighboring AUV is a practical case that often occurs in the leader-follower formation framework. A collaborative nonlinear protocol is applied in (Yuan et al., 2019), and an observer based on the consensus principle is utilized in (Yuan et al., 2018) to estimate the leader's state.

This paper focuses on the cooperative learning formation control problem based on position estimation for a group of AUVs with uncertainties and disturbances under the finite-time prescribed performance control framework. Specifically, two distinct control laws are employed for the leader and followers. The trajectory-following control law for the leader achieves independent control of the velocity while ensuring accurate tracking by using the parametric path. The position of the leader is assumed to be available only for the leader's neighboring AUV, and a finite-time distributed observer (FTDO) is presented for the followers to estimate the leader's position in a finite time. Based on this, the leader-follower control law for followers is derived in which the model uncertainties are learned in a cooperative way using deterministic learning techniques and the experience gained from the learning will be utilized to construct an empirically based formation control law. The finite-time prescribed performance control (FTPPC) approach is imported into the control law design to ensure that the errors converge in a finite time, which speeds up the learning process.

The contributions of this article can be generalized as follows:

- (1) In contrast to the control law proposed in (Fei et al., 2022; Liu et al., 2021a), in which the tracking path is time-related, the parameterized path presented in this paper enables the velocity of the AUVs to be specified independently while accurately tracking the reference trajectory.
- (2) Compared to the RBFNN used in (Wu and Huang, 2022; Zong et al., 2021), the localized RBFNNs used in this paper learn the uncertainties in a cooperative way, and the knowledge obtained from learning is used to construct an empirically based control law to deal with similar uncertainties using experience instead of repeatedly using adaptive methods, which reduces the computing burden.
- (3) Compared to the control law in (Gao and Guo, 2020; Huang et al., 2021), which is derived based on the assumption that all followers have access to the leader's state, in this paper, the position of the leader is assumed to be available only for the leader's neighboring AUV, and a finite-time distributed observer is proposed for the followers to estimate the leader's position in a finite time.
- (4) In contrast to the existing cooperative learning control law (Dai et al., 2022), the control law proposed in this paper is derived from the finite-time prescribed performance control method. A finite-time performance function is used for the error transformation, which allows the error to converge in finite time rather than in the traditional exponential decay way, which speed up cooperative learning process.

The remainder of this paper is organized as follows. Sect. 2 presents the preliminaries. Formation control law design is given in Sect. 3. The empirically based formation control law is provided in Sect. 4. Simulation results are provided in Sect. 5. Sect. 6 concludes the article.

The following notation is used in this article. $\mathbf{1}_n = [1, \dots, 1] \in \mathbb{R}^n$, $\text{sgn}(m) = \text{sgn}(m)|m|^\alpha$, and $A \otimes B$ refer to the Kronecker product. $\|a\|_1 = \sum_{i=1}^n |a_i|$, $\|a\|_2 = \sqrt{a^T a}$ and $\|a\|_\infty = \max_{i=1, \dots, n} \{|a_i|\}$ denote the 1-norm, 2-norm, and ∞ -norm of vector a , respectively. To simplify the expression, we state that $\|a\|$ denotes the 2-norm of vector a without causing confusion. $\underline{\lambda}(\cdot)$ and $\bar{\lambda}(\cdot)$ represent the minimum and maximum eigenvalues, respectively.

2. Preliminaries

2.1. Dynamics and formation configuration

We investigate a multi-agent system consisting of $N + 1$ AUVs with uncertain dynamics and external disturbance, which is represented as

$$\begin{aligned} \dot{\eta}_i &= J(\eta_i)\nu_i \\ \dot{\nu}_i &= -C(\nu_i)\nu_i - D(\nu_i)\nu_i - \Delta(\eta_i, \nu_i) + \tau_{d,i} + \tau_i \end{aligned} \quad (1)$$

where i denotes the i – th AUV, $i = [0, 1, \dots, N]$ with 0 stands for the leader and $1, \dots, N$ signifies the followers. $\eta_i = [x_i, y_i, z_i, \varphi_i, \theta_i, \psi_i]^T$ indicates the position and heading declination in the earth-fixed frame, $\nu_i = [u_i, v_i, w_i, p_i, q_i, r_i]^T$ represents the velocities in the body-fixed frame, $J(\eta_i)$ stands for the rotation matrix, the model matrices M , $C(\nu_i)$, $D(\nu_i)$ and $\Delta(\eta_i, \nu_i)$ denote inertia, Coriolis, damping and unmodeled dynamics, respectively, $\tau_{d,i}$ and τ_i stand for the disturbance and control input, respectively.

The parametric trace path for the leader is depicted by

$$\eta_{r,0}(\sigma) = [x_{r,0}(\sigma), y_{r,0}(\sigma), z_{r,0}(\sigma), \varphi_{r,0}(\sigma), \theta_{r,0}(\sigma), \psi_{r,0}(\sigma)] \quad (2)$$

where $\sigma(t)$ represents the path parameter variable. The trace path of the i – th follower is deduced by $\eta_{r,i} = \eta_0 + \eta_i^*$, where η_i^* refers to the relative position vector.

Remark 1. Unlike the paths with time t as the variable used in the literature (Fei et al., 2022; Shen et al., 2018). In this paper, a parametric path is proposed as a function of the path variable $\sigma(t)$, which indicates that the path can be governed by $\sigma(t)$. Therefore, the velocity can be independently designed from trajectory tracking.

2.2. Graph theory

Consider a graph $\mathcal{G} = (\mathcal{V}, \mathcal{E}, \mathcal{A}, \mathcal{L})$, where $\mathcal{V} = \{b_1, \dots, b_n\}$ stands for the node set, $\mathcal{E} \subseteq \{(b_i, b_k) | b_i, b_k \in \mathcal{V}, b_i \neq b_k\}$ represents the edge set, and the neighbor set of node b_i is specified by $\mathcal{N}_i = \{b_k \in \mathcal{V}, (b_k, b_i) \in \mathcal{E}\}$. The weighted adjacency matrix of \mathcal{G} is represented as $\mathcal{A} = [a_{ik}]$ with $a_{ik} > 0$ if $(b_i, b_k) \in \mathcal{E}$; otherwise, $a_{ik} = 0$. The Laplacian matrix \mathcal{L} is defined by $\mathcal{L} = [l_{ik}]$, where $l_{ii} = \sum_{k \in \mathcal{N}_i} a_{ik}$, $l_{ik} = -a_{ik}$. Moreover, if $(b_i, b_k) \in \mathcal{E} \Leftrightarrow (b_k, b_i) \in \mathcal{E}$, \mathcal{G} is a directed graph; otherwise, \mathcal{G} is an undirected graph.

2.3. Communication topology

Let communication topology among the leader-followers multi-AUV system be described by graph theory with the leader marked as 0 and the followers tagged as $1, \dots, n$. The communication among followers is specified by an undirected graph $\mathcal{G}_1 = (\mathcal{V}_1, \mathcal{E}_1, \mathcal{A}_1, \mathcal{L}_1)$. The communication for the whole AUVs system can be established by directed graph $\mathcal{G}_2 = (\mathcal{V}_2, \mathcal{E}_2, \mathcal{A}_2, \mathcal{L}_2)$ with $\mathcal{V}_2 = \mathcal{V}_1 \cup \{0\}$. $\mathcal{C} = \text{diag}[c_1, \dots, c_n]$ is considered to be the leader weighted adjacency matrix of \mathcal{G}_2 .

2.4. RBFNN

In this essay, RBFNN is applied to approximate unknown function

$$f(x) = W^* S(x) + \varepsilon \quad (3)$$

where $W^* = [W_1^*, \dots, W_q^*]^T$ represents the optimal weight, ε stands for the inherent error that satisfies $|\varepsilon| \leq \bar{\varepsilon}$ with $\bar{\varepsilon}$ maintaining a small value, and $S(x) = [s_1(x), \dots, s_q(x)]^T$ denotes the basis function, where q is the quantity of nodes and $s_i(x)$ is the Gauss activation function.

$$s_i(x) = \exp\left(-\frac{\|x - \mu_i\|_2^2}{\sigma^2}\right) \quad (4)$$

where μ_i and σ stand for the center and base width, respectively.

The control law is devised under the following assumptions:

Assumption 1. The graph contains at least one directed spanning tree with node 0 as its root.

Assumption 2. The communication graph $\mathcal{G}_1 = (\mathcal{V}_1, \mathcal{E}_1, \mathcal{A}_1, \mathcal{L}_1)$ is connected.

Assumption 3. The disturbance $\tau_{d,i}$ is limited by the unknown bound.

Assumption 4. The leader's parametric trace path $\eta_{r,0}(\sigma)$ and its derivative with respect to time $\dot{\eta}_{r,0}$, $\ddot{\eta}_{r,0}$ are periodic and bounded. Meanwhile, $\partial\eta_{r,0}/\partial\sigma$ and $\partial^2\eta_{r,0}/\partial\sigma^2$ are bounded.

The control objectives are stated as follows:

- 1) Design the trajectory-following control law for the leader to achieve accurate tracking along the parameterized path and guarantee that the path update rate converges to a given value simultaneously.
- 2) Design the leader-following control law for followers to realize accurate tracking to the leader. On this basis, the knowledge gained from the adaptive process is applied to design an empirically based control law to enhance control properties.

3. Formation control law design

3.1. Trajectory-following control for the leader

The dynamics model for the leader can be reformulated as

$$\begin{aligned} \dot{\eta}_0 &= J(\eta_0)\nu_0 \\ \dot{\nu}_0 &= \chi_0 + M^{-1}\tau_0 \end{aligned} \quad (5)$$

where $\chi_0 = M^{-1}[-C(\nu_0)\nu_0 - D(\nu_0)\nu_0 - \Delta(\eta_0, \nu_0) + \tau_{d,0}]$ indicates the lumped uncertainty, which is estimated using the FTESO in this paper.

$$\begin{aligned} \dot{\hat{\eta}}_0 &= -\frac{3}{m}J(\eta_0)\text{sig}^{\beta_1}(m^2J^T(\eta_0)\tilde{\eta}_0) + J(\eta_0)\hat{\nu}_0 \\ \dot{\hat{\nu}}_0 &= -3\text{sig}^{2\beta_1-1}(m^2J^T(\eta_0)\tilde{\eta}_0) + \hat{\chi}_0 + M^{-1}\tau_0 \\ \dot{\hat{\chi}}_0 &= -m\text{sig}^{3\beta_1-2}(m^2J^T(\eta_0)\tilde{\eta}_0) \end{aligned} \quad (6)$$

where m represents the observer gain and $\beta_1 \in (0, 1)$ refers to the adjustment parameter. $\hat{\eta}_0$, $\hat{\nu}_0$ and $\hat{\chi}_0$ stand for the estimation of η_0 , ν_0 and χ_0 , respectively, with the estimation error calculated as $(\bullet) = (\bullet) - (\bullet)$. Defining the observer error variable $\varpi_1(t) = m^2\tilde{\eta}(t/m)$, $\varpi_2(t) = m\tilde{\nu}(t/m)$, $\varpi_3(t) = \tilde{\chi}_0(t/m)$, the error system can then be stated as

$$\begin{aligned} \dot{\varpi}_1(t) &= -3J(\eta_0)\text{sig}^{\beta_1}(J^T(\eta_0)\varpi_1(t)) + J(\eta_0)\varpi_2(t) \\ \dot{\varpi}_2(t) &= -3\text{sig}^{2\beta_1-1}(J^T(\eta_0)\varpi_1(t)) + \varpi_3(t) \\ \dot{\varpi}_3(t) &= -\text{sig}^{3\beta_1-2}(J^T(\eta_0)\varpi_1(t)) - \dot{\chi}_0/m \end{aligned} \quad (7)$$

According to the analysis in (Liu et al., 2019), it is evident that (7) will converge in finite time so that the estimation errors converge in finite time.

Step 1

The tracking error of the leader is given by $x_{1,0} = \eta_0(t) - \eta_{r,0}(\sigma)$ and its derivative is

$$\dot{x}_{1,0} = J(\eta_0)\nu_0 - \frac{\partial\eta_{r,0}(\sigma)}{\partial\sigma}(\mathcal{I} - \mathcal{P}) \quad (8)$$

where \mathcal{I} represents the desired path update rate, and \mathcal{P} is an auxiliary variable satisfying $\mathcal{P} = \mathcal{I} - \dot{\sigma}$.

The virtual control law α_0 is devised as follows:

$$\alpha_0 = -K_{1,0}J^T(\eta_0)x_{1,0} + J^T(\eta_0)\frac{\partial\eta_{r,0}(\sigma)}{\partial\sigma}\mathcal{I} \quad (9)$$

where $K_{1,0}$ is the positive definite gain diagonal matrix.

The update law is designed as

$$\dot{\mathcal{P}} = -\left(\mathcal{P} + k_{\mathcal{P}}x_{1,0}\left(\frac{\partial\eta_{r,0}(\sigma)}{\partial\sigma}\right)^T\right) \quad (10)$$

where $k_{\mathcal{P}} > 0$ is the design gain.

Step 2

The error variable $x_{2,0}$ is considered to be $x_{2,0} = \hat{\nu}_0 - \alpha_0$. Its derivative is formulated as

$$\dot{x}_{2,0} = -3\text{sig}^{2\beta_1-1}(m^2J^T(\eta_0)\tilde{\eta}_0) + \hat{\chi}_0 + M^{-1}\tau_0 - \dot{\alpha}_0 - \dot{\hat{\nu}}_0 \quad (11)$$

The trajectory-following control law for the leader is given by

$$\tau_0 = M(-K_{2,0}x_{2,0} - J^T(\eta_0)x_{1,0} - \hat{\chi}_0 + 3\text{sig}^{2\beta_1-1}(m^2J^T(\eta_0)\tilde{\eta}_0) + \dot{\alpha}_0) \quad (12)$$

where $K_{2,0}$ is the positive definite gain diagonal matrix.

Theorem 1. For the leader whose dynamic can be described by (1) in the multi-AUV system with the parametric path given by (2), the FTESO designed as (Eqn 6), control laws described by (12), and update law given by (10), the following conclusions hold. (i) The state variables are UUB. (ii) The path-tracking velocity can be designed independently.

Proof:

Consider the following Lyapunov function:

$$V_0 = \frac{1}{2}x_{1,0}^T x_{1,0} + \frac{1}{2}x_{2,0}^T x_{2,0} + \frac{1}{2k_{\mathcal{P}}} \mathcal{P}^2 \quad (13)$$

whose derivative can be inferred as follows given (8), (10), (11) and (12):

$$\begin{aligned} \dot{V}_0 &= x_{1,0}^T \left(-K_{1,0}x_{1,0} + J(\eta_0)x_{2,0} - J(\eta_0)\hat{\nu}_0 + \frac{\partial\eta_{r,0}(\sigma)}{\partial\sigma}\mathcal{P} \right) \\ &\quad + x_{2,0}^T \left(-K_{2,0}x_{2,0} - J^T(\eta_0)x_{1,0}^T \right) - \frac{1}{k_{\mathcal{P}}} \mathcal{P} \left(\mathcal{P} + k_{\mathcal{P}}x_{1,0}\left(\frac{\partial\eta_{r,0}(\sigma)}{\partial\sigma}\right)^T \right)^T \\ &= -x_{1,0}^T K_{1,0}x_{1,0} - x_{2,0}^T K_{2,0}x_{2,0} - \frac{1}{k_{\mathcal{P}}} \mathcal{P}^2 - x_{1,0}^T J(\eta_0)\hat{\nu}_0 \\ &\leq -x_{1,0}^T K_{1,0}x_{1,0} - x_{2,0}^T K_{2,0}x_{2,0} - \frac{1}{k_{\mathcal{P}}} \mathcal{P}^2 + \|x_{1,0}\| \|\hat{\nu}_0\| \\ &\leq -\varsigma_0 V_0 + \kappa_0 \end{aligned} \quad (14)$$

where $\varsigma_0 = \min\{2\lambda(K_{1,0}), 2\lambda(K_{2,0}), 2\}$, $\kappa_0 = \|x_{1,0}\| \|\hat{\nu}_0\|$.

Based on (14), we obtain $V_0 \leq V_0(0)e^{-\varsigma_0 t} + \mathcal{C}_0$, from which the following statement holds.

$$\|x_{1,0}\| \leq \sqrt{2\mathcal{C}_0}, \|x_{2,0}\| \leq \sqrt{2\mathcal{C}_0}, \|\mathcal{P}\| \leq \sqrt{2k_{\mathcal{P}}\mathcal{C}_0} \quad (15)$$

where $\mathcal{C}_0 = \kappa_0/\varsigma_0$ depicts the adjustable compact set.

According to (15), $x_{1,0}$, $x_{2,0}$ and \mathcal{P} are bounded, and based on (9) and Assumption 4, α_0 and $\dot{\alpha}_0$ are bounded. Further analysis reveals that $\dot{x}_{1,0}$ and $\dot{x}_{2,0}$ are bounded since the lumped uncertainty χ_0 is bounded according to Assumption 3. This ends the proof. ■

3.2. Finite-time distributed observer

From [Assumption 1](#), not all followers can reap the information sent by the leader, implying that the leader's position is not accessible for all the followers. This entails information exchange between AUV followers to collaboratively estimate the leader's position. To address this problem, based on the consensus principle and finite time theory, a finite-time distributed observer is proposed as follows

$$\begin{aligned}\dot{\tilde{\eta}}_0^i &= -k_1 \text{sig}^{\beta_2} \left(\sum_{j=1}^n a_{ij} (\tilde{\eta}_0^i - \tilde{\eta}_0^j) + c_i (\tilde{\eta}_0^i - \eta_0) \right) \\ &\quad - k_2 \text{sgn} \left(\sum_{j=1}^n a_{ij} (\tilde{\eta}_0^i - \tilde{\eta}_0^j) + c_i (\tilde{\eta}_0^i - \eta_0) \right)\end{aligned}\quad (16)$$

where $\tilde{\eta}_0^i$ stands for the i -th follower's estimation of η_0 , and $\beta_2 \in (0, 1)$, $k_1 > 0$, and $k_2 > \|\dot{\eta}_0\|_\infty$ are the observer parameters.

Lemma 1.

$$\dot{x} = f(x), f(0) = 0, x \in \mathbb{R}^n \quad (17)$$

For system (17), if there is a continuous function $V(x) > 0$ that meets $\dot{V}(x) \leq -kV(x)^m$, where $k > 0$, $0 < m < 1$, $x \in \mathbb{R}^n$ and $x \neq 0$, then we can derive that system (17) will converge to 0 in finite time T , which can be determined as $T \leq \frac{V^{1-m}(x(0))}{k(1-m)}$.

$$T_1 = \min \left\{ \frac{2^{(1-\beta_2)/2} (6n)^{\beta_2} \bar{\lambda}^{(1+\beta_2)/2} (\mathcal{L}_1 + \mathcal{C}) V_{ob}(0)^{(1-\beta_2)/2}}{(1-\beta_2) k_1 \underline{\lambda}^{1+\beta_2} (\mathcal{L}_1 + \mathcal{C})}, \frac{2^{1/2} \bar{\lambda}^{1/2} (\mathcal{L}_1 + \mathcal{C}) V_{ob}(0)^{1/2}}{(k_2 - \|\dot{\eta}_{0L}\|_\infty) \underline{\lambda} (\mathcal{L}_1 + \mathcal{C})} \right\} \quad (26)$$

Lemma 2. For multi-agent systems in the leader-followers framework, if [Assumption 1](#) holds, then $\mathcal{L}_1 + \mathcal{C}$ is positive definite.

Theorem 2. The estimation error of the observer ([Eqn 16](#)) converges in finite time given that [Assumption 1](#) holds and $\dot{\eta}_0$ is bounded.

Proof:

The estimation error $\tilde{\eta}_0^i$ and the error vector $\tilde{\eta}_0$ are given as $\tilde{\eta}_0^i = \tilde{\eta}_0^i - \eta_0$ and $\tilde{\eta}_0 = [\tilde{\eta}_0^1, \dots, \tilde{\eta}_0^n]^T$, respectively.

The Lyapunov function is given by

$$V_{ob} = \frac{1}{2} \tilde{\eta}_0^T ((\mathcal{L}_1 + \mathcal{C}) \otimes I_6) \tilde{\eta}_0 \quad (18)$$

Further deduction shows that

$$V_{ob} \leq \bar{\lambda} (\mathcal{L}_1 + \mathcal{C}) \|\tilde{\eta}_0\|_2^2 / 2 \quad (19)$$

Defining $\zeta = [\zeta_1, \dots, \zeta_{6n}]^T = ((\mathcal{L}_1 + \mathcal{C}) \otimes I_6) \tilde{\eta}_0$, [\(18\)](#) can be rewritten as $V_{ob} = 1/2 \tilde{\eta}_0^T \zeta$, whose derivative can be calculated as

$$\begin{aligned}\dot{V}_{ob} &= \zeta^T (-k_1 \text{sig}^{\beta_2}(\zeta) - k_2 \text{sgn}(\zeta) - \mathbf{1}_n \otimes \dot{\eta}_0) \\ &= -k_1 \zeta^T \text{sig}^{\beta_2}(\zeta) - k_2 \|\zeta\|_1 - \zeta^T \dot{\eta}_0\end{aligned}\quad (20)$$

where $\dot{\eta}_{0L} = \mathbf{1}_n \otimes \dot{\eta}_0$. It follows from Herder's inequality that

$$\begin{aligned}\|\zeta\|_1 &= \sum_{i=1}^{6n} (|\zeta_i| \times 1) \\ &\leq \left(\sum_{i=1}^{6n} |\zeta_i|^{1+\beta_2} \right)^{\frac{1}{1+\beta_2}} \left(\sum_{i=1}^{6n} 1^{\frac{1+\beta_2}{\beta_2}} \right)^{\frac{\beta_2}{1+\beta_2}} \\ &= [\zeta^T \text{sig}^{\beta_2}(\zeta)]^{\frac{1}{1+\beta_2}} (6n)^{\frac{\beta_2}{1+\beta_2}}\end{aligned}\quad (21)$$

which can be further deduced to yield the following inequality:

$$\zeta^T \text{sig}^{\beta_2}(\zeta) \geq (6n)^{-\beta_2} \|\zeta\|_1^{1+\beta_2} \quad (22)$$

Using Herder's inequality again yields

$$\begin{aligned}|\zeta^T \dot{\eta}_{0L}| &= \left| \sum_{i=1}^{6n} \zeta_i \dot{\eta}_{0Li} \right| \\ &\leq \left(\sum_{i=1}^{6n} |\zeta_i| \right) \left(\sum_{i=1}^{6n} |\dot{\eta}_{0Li}|^{+\infty} \right)^{\frac{1}{+\infty}} = \|\zeta\|_1 \|\dot{\eta}_{0L}\|_\infty\end{aligned}\quad (23)$$

It can be derived from inequalities [\(20\)](#), [\(22\)](#), and [\(23\)](#) that

$$\begin{aligned}\dot{V}_{ob} &\leq -k_1 (6n)^{-\beta_2} \|\zeta\|_1^{1+\beta_2} - (k_2 - \|\dot{\eta}_{0L}\|_\infty) \|\zeta\|_2 \\ &\leq -k_1 (6n)^{-\beta_2} \|\zeta\|_2^{1+\beta_2} - (k_2 - \|\dot{\eta}_{0L}\|_\infty) \|\zeta\|_2 \\ &\leq -k_1 (6n)^{-\beta_2} \underline{\lambda}^{1+\beta_2} (\mathcal{L}_1 + \mathcal{C}) \|\tilde{\eta}_0\|_2^{1+\beta_2} - (k_2 - \|\dot{\eta}_{0L}\|_\infty) \underline{\lambda} (\mathcal{L}_1 + \mathcal{C}) \|\tilde{\eta}_0\|_2\end{aligned}\quad (24)$$

Incorporating inequality [\(19\)](#), we conclude

$$\begin{aligned}\dot{V}_{ob} &\leq -k_1 2^{(1+\beta_2)/2} (6n)^{-\beta_2} \underline{\lambda}^{1+\beta_2} (\mathcal{L}_1 + \mathcal{C}) \frac{V_{ob}^{(1+\beta_2)/2}}{\bar{\lambda}^{(1+\beta_2)/2} (\mathcal{L}_1 + \mathcal{C})} \\ &\quad - 2^{1/2} (k_2 - \|\dot{\eta}_{0L}\|_\infty) \underline{\lambda} (\mathcal{L}_1 + \mathcal{C}) \frac{V_{ob}^{1/2}}{\bar{\lambda}^{1/2} (\mathcal{L}_1 + \mathcal{C})}\end{aligned}\quad (25)$$

Under [Lemma 1](#), $\tilde{\eta}_0^i$ will tend to 0 in finite time T_1 , which is considered to be

The proof ends here. ■

3.3. Leader-following control for followers

The reference tracking trajectory of the i -th follower is given as $\tilde{\eta}_{r,i} = \tilde{\eta}_0^i + \eta_i^*$, where $\tilde{\eta}_0^i$ is obtained by the observer [\(16\)](#). The trace error can be determined as $e_{1,i} = \eta_i - \tilde{\eta}_{r,i} = [e_{1,i1}, \dots, e_{1,i6}]^T$.

$$e_{1,i} = \eta_i - \tilde{\eta}_{r,i} = [e_{1,i1}, \dots, e_{1,i6}]^T \quad (27)$$

In the PPC framework, the error transformation can be characterized as

$$e_{1,ij} = h_{ij}(t) G_{ij}(x_{1,ij}) \quad (28)$$

where G_{ij} refers to the error transformation function and $x_{1,ij}$ is the conversion error:

$$G_{ij}(x_{1,ij}) = \frac{\exp(x_{1,ij}) - \exp(-x_{1,ij})}{\exp(x_{1,ij}) + \exp(-x_{1,ij})} \quad (29)$$

$h_{ij}(t)$ stands for the performance function that constrains $e_{1,ij}$ to converge in a finite time:

$$h_{ij}(t) = \begin{cases} \left(h_{ij}(0) - \frac{t}{T_{2,i}} \right) \exp \left(1 - \frac{T_{2,i}}{T_{2,i} - t} \right) + h_{ij}(\infty), & 0 \leq t < T_{2,i} \\ h_{ij}(\infty), & t \geq T_{2,i} \end{cases} \quad (30)$$

where $T_{2,i}$ is the preset time, $h_{ij}(0) > 1$ and $h_{ij}(\infty) > 0$ are parameters for limiting the overshoot and steady-state error, respectively.

Theorem 3. The $h_{ij}(t)$ identified by [\(30\)](#) is a finite-time performance function capable of converging to the final value in a predetermined amount

of time.

Proof:

First, the derivative of (30) is given below:

$$\dot{h}_{ij}(t) = \begin{cases} -\frac{1}{T_{2,i}} \exp\left(1 - \frac{T_{2,i}}{T_{2,i}-t}\right) - \frac{h_{ij}(0)T_{2,i}-t}{(T_{2,i}-t)^2} \exp\left(1 - \frac{T_{2,i}}{T_{2,i}-t}\right), & 0 \leq t < T_{2,i} \\ 0, & t \geq T_{2,i} \end{cases} \quad (31)$$

$$\begin{aligned} \tau_i = M &\left(-K_{2,i}x_{2,i} - J^T(\eta_i)\mathcal{M}_i^T x_{1,i} + \widehat{W}_i^T S(Y_i) - \widehat{\tau}_{D,i}^* \tanh\left(\frac{\widehat{\tau}_{D,i}^* x_{2,i}}{s}\right) + \frac{\partial J^T}{\partial \eta_i} J\nu_i (\mathcal{M}_i^{-1} \Xi_i e_{1,i} - \mathcal{M}_i^{-1} K_{1,i} x_{1,i} + \dot{\hat{\eta}}_{r,i}) \right. \\ &\left. + J^T \left(\mathcal{M}_i^{-1} (\dot{\Xi}_i e_{1,i} + \Xi_i \dot{e}_{1,i} - K_{1,i} \dot{x}_{1,i}) + \dot{\mathcal{M}}_i^{-1} (\Xi_i e_{1,i} - K_{1,i} x_{1,i}) + \ddot{\hat{\eta}}_{r,i} \right) \right) \end{aligned} \quad (38)$$

The calculation reveals that $\dot{h}_{ij}(t) < 0$ when $0 \leq t < T_{2,i}$ from $h_{ij}(0) > 1$, which suggests that $h_{ij}(t)$ is monotonically decreasing. In addition, the calculation shows $h_{ij}(T_{2,i}) \rightarrow h_{ij}(\infty)$, which indicates that $h_{ij}(t)$ decreases monotonically to $h_{ij}(\infty)$ in a preset time $T_{2,i}$.

Furthermore, it can be derived from (31) that $\dot{h}_{ij}(t)$ is continuous in intervals $0 \leq t < T_i$ and $t \geq T_{2,i}$. Further computation shows that $\lim_{t \rightarrow T_{2,i}^-} \dot{h}_{ij}(t) = \lim_{t \rightarrow T_{2,i}^+} \dot{h}_{ij}(t) = \dot{h}_{ij}(T_i) = 0$, which indicates that $\dot{h}_{ij}(t)$ is continuous. This ends the proof. ■

Step 1 Based on (29), the conversion error $x_{1,ij}$ is obtained as

$$x_{1,ij} = \frac{1}{2} \ln \left(1 + \frac{e_{1,ij}}{h_{ij}(t)} \right) - \frac{1}{2} \ln \left(1 - \frac{e_{1,ij}}{h_{ij}(t)} \right) \quad (32)$$

whose derivative is calculated as follows according to (1) and (27):

$$\dot{x}_{1,ij} = \mathcal{M}_i (J(\eta_i) \nu_i - \dot{\hat{\eta}}_{r,i}) - \Xi_i e_{1,i} \quad (33)$$

where $x_{1,i} = [x_{1,i1}, \dots, x_{1,i6}]^T$, $\mathcal{M}_i = \text{diag}[c_{i1}, \dots, c_{i6}]$ and $\Xi_i = \text{diag}[g_{i1}, \dots, g_{i6}]$, c_{ij} and g_{ij} are given by

$$\begin{aligned} c_{ij} &= \frac{1}{2} \left(\frac{1}{h_{ij}(t) + e_{1,ij}} + \frac{1}{h_{ij}(t) - e_{1,ij}} \right) \\ g_{ij} &= \frac{1}{2} \left(\frac{\dot{h}_{ij}(t)}{h_{ij}(t)(h_{ij}(t) + e_{1,ij})} + \frac{\dot{h}_{ij}(t)}{h_{ij}(t)(h_{ij}(t) - e_{1,ij})} \right) \end{aligned} \quad (34)$$

The virtual control law α_i is specified by

$$\alpha_i = J^T(\eta_i) (-\mathcal{M}_i^{-1} K_{1,i} x_{1,i} + \dot{\hat{\eta}}_{r,i} + \mathcal{M}_i^{-1} \Xi_i e_{1,i}) \quad (35)$$

Step 2 The error variable is classified as $x_{2,i} = \nu_i - \alpha_i$, whose derivative is calculated as

$$\begin{aligned} \dot{x}_{2,i} &= -M^{-1} [C(\nu_i) \nu_i + D(\nu_i) \nu_i + \Delta(\eta_i, \nu_i)] + M^{-1} \tau_i + \tau_{M,i} \\ &\quad - \frac{\partial J^T}{\partial \eta_i} J\nu_i (\mathcal{M}_i^{-1} \Xi_i e_{1,i} - \mathcal{M}_i^{-1} K_{1,i} x_{1,i} + \dot{\hat{\eta}}_{r,i}) \\ &\quad - J^T \left(\mathcal{M}_i^{-1} (\dot{\Xi}_i e_{1,i} + \Xi_i \dot{e}_{1,i} - K_{1,i} \dot{x}_{1,i}) + \dot{\mathcal{M}}_i^{-1} (\Xi_i e_{1,i} - K_{1,i} x_{1,i}) + \ddot{\hat{\eta}}_{r,i} \right) \end{aligned} \quad (36)$$

where $\tau_{M,i} = M^{-1} \tau_{d,i}$ stands for the disturbance term that satisfies $|\tau_{M,i}| \leq \tau_{d,i}^*$ with $\tau_{d,i}^*$ being an unknown constant vector. Let $F_i(Y_i) =$

$M^{-1} [C(\nu_i) \nu_i + D(\nu_i) \nu_i + \Delta(\eta_i, \nu_i)] = [f_{1i}(Y_i), \dots, f_{16}(Y_i)]^T$ be the total uncertainty, which can be approximated by RBFNN.

$$f_{ij}(Y_i) = W_{ij}^T S_j(Y_i) + \varepsilon_{ij} \quad (37)$$

where $Y_i = [\eta_i^T, \nu_i^T]^T \in \mathbb{R}^{12}$.

The control law is formulated as

where \widehat{W}_i^T is the estimation of W_i^T with $W_i^* = \text{blockdiag}[W_{1i}^T, \dots, W_{16i}^T] \in \mathbb{R}^{6 \times 6q}$, $S(Y_i) = [S_1^T(Y_i), \dots, S_6^T(Y_i)]^T \in \mathbb{R}^{6q}$, $s > 0$, $\widehat{\tau}_{D,i}^* = \text{diag}[\widehat{\tau}_{d,11}^*, \dots, \widehat{\tau}_{d,16}^*]$, and $\widehat{\tau}_{d,ij}^*$ represents the estimate of $\tau_{d,ij}^*$ whose update law is conceived as

$$\dot{\widehat{\tau}}_{d,ij}^* = \gamma_d \left(\mu_{d,ij} \widehat{\tau}_{d,ij}^* + |x_{2,ij}| \right) \quad (39)$$

where $\gamma_d > 0$, and $\mu_{d,ij} > 0$ are the design parameters.

Remark 2. Compared to (Yuan et al., 2018, 2019), which did not account for external disturbances, in this work, the adaptive strategy is employed to estimate the disturbance, and the results are applied to the control law in a novel way to compensate for disturbance. In addition, the strategy proposed in this article achieves a more accurate estimation compared to the approach using NN since the disturbances vary only with time independent of other factors, therefore, the input to NN is not available.

The update law of \widehat{W}_i is given by

$$\dot{\widehat{W}}_{ij} = \Lambda_{1,ij} \left(-S_j(Y_i) x_{2,ij} + \mu_{W,ij} \widehat{W}_{ij} \right) - k_{W,ij} \sum_{k=1}^N a_{ik} (\widehat{W}_{ij} - \widehat{W}_{kj}) \quad (40)$$

where $\Lambda_{1,ij}$ represents the positive definite gain matrix to be designed, $\mu_{W,ij}$ and $k_{W,ij}$ are positive constants, $\Lambda_{1,ij} \left(-S_j(Y_i) x_{2,ij} + \mu_{W,ij} \widehat{W}_{ij} \right)$ is the adaptive term and $k_{W,ij} \sum_{k=1}^N a_{ik} (\widehat{W}_{ij} - \widehat{W}_{kj})$ is the cooperative term.

Remark 3. In contrast to the RBFNN mentioned in papers (Cui et al., 2017b; Fei et al., 2022), which is extensively used in formation control laws, the introduction of the cooperative term makes it possible for each AUV to share the estimation of uncertainty gained through the adaptive method with its neighbor AUVs. Therefore, the RBFNN with the cooperative term added has better generalization capability and is more suitable for the AUVs formation control problem.

Theorem 4. For followers whose dynamic can be described by (1) in the multi-AUV system with distributed observers designed as (Eqn 16), the control law described by (38), and the update laws given by (39) and (40), the following conclusions hold. (i) The state variables are all UUB. (ii) The tracking error $e_{1,ij}$ is constrained by $h_{ij}(t)$ and converges to the adjustable compact set in a finite time.

Proof:

The Lyapunov function is given by

$$V_{1,i} = \frac{1}{2} \dot{x}_{1,i}^T x_{1,i} + \frac{1}{2} \dot{x}_{2,i}^T x_{2,i} + \frac{1}{2} \sum_{j=1}^6 \tilde{W}_{ij}^T \Lambda_{1,j}^{-1} \tilde{W}_{ij} + \frac{1}{2} \gamma_d^{-1} \sum_{j=1}^6 \tilde{\tau}_{d,ij}^{*2} \quad (41)$$

where $\tilde{W}_{ij} = W_{ij}^* - \widehat{W}_{ij}$ and $\tilde{\tau}_{d,ij}^* = \tau_{d,ij}^* - \widehat{\tau}_{d,ij}^*$. Combining (33), (36), (38), (39) and (40), $\dot{V}_{1,i}$ can be determined as

$$\begin{aligned} \dot{V}_{1,i} &= x_{1,i}^T (-K_{1,i} x_{1,i} + \mathcal{M}_i \mathcal{J}(\eta_i) x_{2,i}) - \sum_{j=1}^6 \tilde{\tau}_{d,ij}^* (\mu_{d,ij} \widehat{\tau}_{d,ij}^* + |x_{2,ij}|) \\ &+ x_{2,i}^T \left(-K_{2,i} x_{2,i} - J^T(\eta_i) \mathcal{M}_i^T x_{1,i} - \tilde{W}_{ij}^T S(\Upsilon_i) - \varepsilon_i + \tau_{M,i} - \widehat{\tau}_{D,i}^* \tanh\left(\frac{\widehat{\tau}_{D,i}^* x_{2,i}}{s}\right) \right) \\ &- \sum_{j=1}^6 \tilde{W}_{ij}^T (-S_j(\Upsilon_i) x_{2,ij} + \mu_{W,ij} \widehat{W}_{ij}) - \sum_{j=1}^6 \Lambda_{1,j}^{-1} k_{W,j} \tilde{W}_{ij}^T (\mathcal{L}_1 \otimes I) \tilde{W}_{ij} \\ &= -x_{1,i}^T K_{1,i} x_{1,i} - x_{2,ij}^T K_{2,i} x_{2,i} - x_{2,ij}^T \varepsilon_i \\ &- \sum_{j=1}^6 \left(\mu_{W,ij} \tilde{W}_{ij}^T \widehat{W}_{ij} + \mu_{d,ij} \tilde{\tau}_{d,ij}^* \widehat{\tau}_{d,ij}^* \right) - \sum_{j=1}^6 \Lambda_{1,j}^{-1} k_{W,j} \tilde{W}_{ij}^T (\mathcal{L}_1 \otimes I) \tilde{W}_{ij} \\ &+ \sum_{j=1}^6 \left(x_{2,ij} \tau_{M,ij} - |x_{2,ij}| \tau_{d,ij}^* + |x_{2,ij}| \widehat{\tau}_{d,ij}^* - x_{2,ij} \widehat{\tau}_{d,ij}^* \tanh\left(\frac{x_{2,ij} \widehat{\tau}_{d,ij}^*}{s}\right) \right) \end{aligned} \quad (42)$$

where $k_{W,j} = \text{diag}[k_{W,ij}, \dots, k_{W,Nj}]$ and $\Lambda_{1,j}^{-1} = \text{diag}[\Lambda_{1,1j}^{-1}, \dots, \Lambda_{1,Nj}^{-1}]$ are the positive definite matrix, and $\widetilde{W}_j = [\tilde{W}_{1j}^T, \dots, \tilde{W}_{Nj}^T]^T$. According to **Assumption 2**, \mathcal{L}_1 is semi-positive definite, which leads to $\sum_{j=1}^6 \Lambda_{1,j}^{-1} k_{W,j} \widetilde{W}_j^T (\mathcal{L}_1 \otimes I) \widetilde{W}_j > 0$. Further analysis shows that $x_{2,ij} \tau_{M,ij} \leq |x_{2,ij}| \tau_{d,ij}^*$ and $|x_{2,ij}| \widehat{\tau}_{d,ij}^* \leq |x_{2,ij}| \widehat{\tau}_{d,ij}^*$, which leads to

$$x_{2,ij} \tau_{M,ij} - |x_{2,ij}| \tau_{d,ij}^* + |x_{2,ij}| \widehat{\tau}_{d,ij}^* - x_{2,ij} \widehat{\tau}_{d,ij}^* \tanh\left(\frac{x_{2,ij} \widehat{\tau}_{d,ij}^*}{s}\right) \leq 0.2785s \quad (43)$$

exploiting the hyperbolic tangent function characteristic $0 \leq |m| - m \tanh(m/s) \leq 0.2785s$.

From Young's inequality, we get

$$\begin{aligned} -\mu_{W,ij} \tilde{W}_{ij}^T \widehat{W}_{ij} &\leq -\frac{\mu_{W,ij} \|\tilde{W}_{ij}\|^2}{2} + \frac{\mu_{W,ij} \|W_{ij}^*\|^2}{2} \\ -\mu_{d,ij} \tilde{\tau}_{d,ij}^* \widehat{\tau}_{d,ij}^* &\leq -\frac{\mu_{d,ij} \|\tilde{\tau}_{d,ij}^*\|^2}{2} + \frac{\mu_{d,ij} \|\tau_{d,ij}^*\|^2}{2} \\ -x_{2,i}^T \varepsilon_i &\leq \frac{\|x_{2,i}\|^2}{2} + \frac{\|\bar{\varepsilon}_i\|^2}{2} \end{aligned} \quad (44)$$

Combining the above inequalities reveals that

$$\begin{aligned} \dot{V}_{1,i} &\leq - \left(x_{1,i}^T K_{1,i} x_{1,i} + x_{2,i}^T K_{2,i} x_{2,i} - \frac{\|x_{2,i}\|^2}{2} + \sum_{j=1}^6 \frac{\mu_{W,ij} \|\tilde{W}_{ij}\|^2}{2} + \frac{\mu_{d,ij} \|\tilde{\tau}_{d,ij}^*\|^2}{2} \right) \\ &+ \left(\frac{\|\bar{\varepsilon}_i\|^2}{2} + \sum_{j=1}^6 \left(\frac{\mu_{W,ij} \|W_{ij}^*\|^2}{2} + \frac{\mu_{d,ij} \|\tau_{d,ij}^*\|^2}{2} \right) \right) + 1.671s \\ &\leq -\varsigma_1 V_{1,i} + \kappa_1 \end{aligned} \quad (45)$$

where $\varsigma_1 = \min\{2\lambda(K_{1,i}), 2\lambda(K_{2,i}) - 1, \mu_{W,ij}\lambda(\Lambda_{1,ij}), \mu_{d,ij}\gamma_d\}$, $\kappa_1 = (\|\bar{\varepsilon}_i\|^2/2 + \sum_{j=1}^6 (\mu_{W,ij} \|W_{ij}^*\|^2/2 + \mu_{d,ij} \|\tau_{d,ij}^*\|^2/2) + 1.671s)$.

According to (45), we can deduce $V_{1,i} \leq V_{1,i}(0)e^{-\varsigma_1 t} + \mathcal{Q}_1$, which means that the following result stands

$$\begin{aligned} \|x_{1,i}\| &\leq \sqrt{2\mathcal{Q}_1}, \|x_{2,i}\| \leq \sqrt{2\mathcal{Q}_1}, \|\tilde{W}_{ij}\| \leq \sqrt{2\mathcal{Q}_1/\lambda(\Lambda_{1,ij})}, |\tilde{\tau}_{d,ij}^*| \\ &\leq \sqrt{2\mathcal{Q}_1\gamma_d} \end{aligned} \quad (46)$$

where $\mathcal{Q}_1 = \kappa_1/\varsigma_1$ indicates an adjustable compact set.

It is evident that $x_{1,i}$, $x_{2,i}$, \tilde{W}_{ij} and $\tilde{\tau}_{d,ij}^*$ are UUB by proper choice of the above parameters. According to (35) and **Assumption 4**, α_i and $\dot{\alpha}_i$ are bounded. Subsequently, $x_{1,i}$ and $x_{2,i}$ are bounded since the dynamic uncertainties are bounded. Therefore, all the state variables are UUB. From (28)–(30) and the convergence of the conversion error $x_{1,i}$, the tracking error $e_{1,i}$ is limited by the performance function and converges in a finite time. ■

4. Empirically based formation control law design

4.1. Learning in the process of tracing tracks

For localized RBFNN, each basis function can impact the output of the NN only regionally. Therefore, localized RBFNN has the potential of learning during the adaptive process.

Lemma 3. Consider $x(t)$ as the continuous periodic signal restricted to a certain bounded set Ω_x . Then, for the RBFNN $W^T S(x)$ whose center satisfies $\mu \in \Omega$ with Ω being large enough to cover Ω_x , the corresponding regressor subvector $S_p(x)$ is persistently exciting (PE).

Theorem 5. For the multi-AUV system whose dynamic is described by (1), the trajectory-following control law for the leader is given in Sect. 3.1, and the leader-following control law for followers is given in Sect. 3.3. If there exists a set Ω_{Y_i} satisfying $Y_i \in \Omega_{Y_i}$ at any moment, then under the premise that $Y_i(0)$ is bounded and $\widehat{W}_{ij}(0) = 0$, we can conclude that the regressor subvector $S_p(Y_i)$ satisfies the partial PE condition.

Proof:

Theorem 1 demonstrates that $x_{1,0}, x_{2,0} \rightarrow 0$ holds by choosing proper parameters, which implies that η_0 and ν_0 are periodic signals combining **Assumption 4**. **Theorem 2** proves that $\widehat{\eta}_0^i \rightarrow \eta_0$ in finite time, further analysis yields that $\widehat{\eta}_{r,i}$ and $\dot{\widehat{\eta}}_{r,i}$ are periodic. **Theorem 4** shows that $e_{1,i}$ and $x_{2,i}$ converge to adjustable compact sets, which demonstrates that η_i and ν_i are periodic according to (27), (35). Therefore, the input of RBFNN $Y_i = [\eta_i^T, \nu_i^T]^T$ is a bounded periodic signal, and hence, the regression subvector $S_p(Y_i)$ satisfies the partial PE condition according to **Lemma 3**. This ends the proof. ■

The properties of localized RBFNNs with regression subvectors satisfying the partial PE condition have been sufficiently discussed and proven in the literature (Wang and Hill, 2006; Wang and Wang, 2015), which means that the following statements hold.

- (i) When the multi-agent system tracks the periodic path accurately, the estimated weight $\widehat{W}_{p,ij}$ for the localized RNFB will converge within a compact set around the optimal value $W_{p,ij}^*$.
- (ii) Accurate approximation of the uncertainty $f_{ij}(Y_i)$ can be realized by $\overline{W}_{ij}^T S_j(Y_i)$ when the multi-agent system accurately tracks the period path, i.e.,

$$f_{ij}(Y_i) = \overline{W}_{ij}^T S_j(Y_i) + \varepsilon_{E,ij} \quad (47)$$

where $\varepsilon_{E,ij}$ denotes the approximation error and \overline{W}_{ij} indicates the experience gained through learning

$$\overline{W}_{ij} = \text{mean } \widehat{W}_{ij}(t), t \geq T_i \quad (48)$$

where $T_i = \inf\{x_{1,0}(t) \leq \iota_1, e_{1,i}(t) \leq \iota_2\}$ and $\iota_1 \rightarrow 0, \iota_2 \rightarrow 0$ refer to the design value.

Remark 4. From the above discussion, it is obvious that learning the uncertainty can start only after the system achieves the steady state, which means that the learning efficiency is affected by the speed of convergence. Compared with (Dai et al., 2022), the FTESO (6), FTDO (16), and FTPPC (28)–(30) employed in this work predetermine the

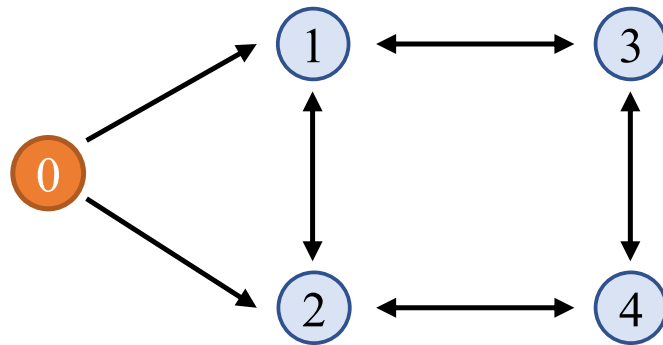


Fig. 1. The communication topology.

Table 1
Parameterized path and initial states.

Items	Values
$\eta_{r,0}$	$\begin{bmatrix} 20 \sin \sigma + 15 \cos \sigma, \\ 15 \sin \sigma - 20 \cos \sigma, \\ 20 \sin \sigma + 15 \cos \sigma, 0, 0, \sigma \end{bmatrix}^T$
$\eta_i(0)$	$\eta_1(0) = [17.5, -20, 16, 1, 1.5, -1]^T$ $\eta_2(0) = [15, -17.5, 17, 1, 1.3, -1]^T$ $\eta_3(0) = [15, -21, 16, 1, -0.5, -1]^T$ $\eta_4(0) = [16, -20, 13, 0.5, -0.5, -1]^T$ $v_i(0) = [0, 0, 0, 0, 0, 0]^T$ $i = 0, \dots, 4$
$v_i(0)$	

convergence time and accelerate the learning progress.

4.2. Empirically based formation control

From (48), the dynamic uncertainties can be learned by RBFNN during the adaptive process, and knowledge will be stored in \bar{W}_{ij} . Using \bar{W}_{ij} , the control law (Eqn 38) can be reframed to an empirically based control law

$$\tau_i = M \left(-K_{2,i} z_{2,i} - J^T(\eta_i) \mathcal{M}_i^T z_{1,i} + \bar{W}_i^T S(Y_i) - \hat{\tau}_{d,i}^* \tanh\left(\frac{\hat{\tau}_{d,i}^* z_{2,i}}{s}\right) + \frac{\partial J^T}{\partial \eta_i} J \nu_i (\mathcal{M}_i^{-1} \Xi_i e_{1,i} - \mathcal{M}_i^{-1} K_{1,i} z_{1,i} + \dot{\hat{\eta}}_{r,i}) \right. \\ \left. + J^T \left(\mathcal{M}_i^{-1} (\dot{\Xi}_i e_{1,i} + \Xi_i \dot{e}_{1,i} - K_{1,i} \dot{z}_{1,i}) + \dot{\mathcal{M}}_i^{-1} (\Xi_i e_{1,i} - K_{1,i} z_{1,i}) + \ddot{\hat{\eta}}_{r,i} \right) \right) \quad (49)$$

Theorem 6. For followers whose dynamic can be described by (1) in the multi-AUV system with distributed observers designed as (Eqn 16), the empirically based control law described by (49), and the update laws given by

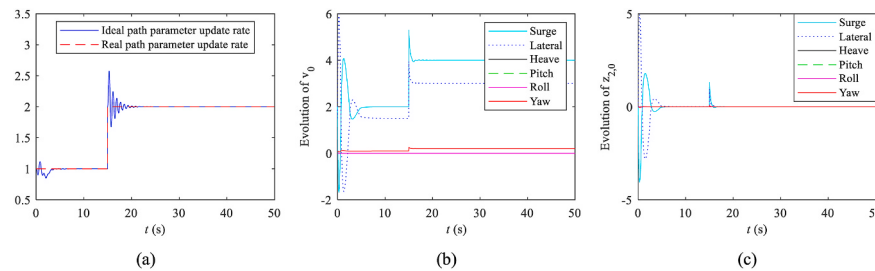


Fig. 2. Control on the velocity using parameterized path. (a) Tracking on the desired path update rate, (b) Velocity evolution of the leader, (c) Velocity error.

Table 2
The parameter values of the control laws.

Parameters	Values
FTESO	$m = 2, \beta_1 = 0.8$
Trajectory-following control law for the leader	$K_{1,0} = \text{diag}[0.5, 0.5, 0.5, 0.5, 0.5, 0.5], K_{2,0} = \text{diag}[5, 5, 5, 5, 5, 5], k_p = 10, \sigma_d = 2\pi/45$
FTDO	$k_1 = 15, k_2 = 5, \beta_2 = 0.6$
FTPPC	$h_{ij}(0) = 4, j = 1, 2, 3,$ $h_{ij}(0) = 2, j = 4, 5, 6,$ $h_{ij}(\infty) = 0.02, T_{2,i} = 20$
Leader-following control law for followers	$K_{1,i} = \text{diag}[0.7, 0.7, 0.7, 0.7, 0.7, 0.7], K_{2,i} = \text{diag}[8, 8, 8, 8, 8], \Lambda_{1,ij} = \text{diag}[6, 6, 6, 6, 6], \mu_{W,ij} = 0.001, k_{W,ij} = 0.1, \mu_{d,ij} = 0.001, s = 0.01, \gamma_d = 0.5$

(39), the following conclusions hold. (i) The state variables are all UUB. (ii) The trace error $e_{1,i}$ converges to an adjustable compact set in a finite time.

Proof:

Construct the following Lyapunov function

$$V_{2,i} = \frac{1}{2} z_{1,i}^T z_{1,i} + \frac{1}{2} z_{2,i}^T z_{2,i} + \frac{1}{2} \gamma_d^{-1} \sum_{j=1}^6 \tilde{\tau}_{d,ij}^2 \quad (50)$$

whose derivative can be calculated as follows combining (33), (36), (38), and (39):

$$\dot{V}_{2,i} = -z_{1,i}^T K_{1,i} z_{1,i} - z_{2,i}^T K_{2,i} z_{2,i} - z_{2,i}^T \varepsilon_{E,i} - \sum_{j=1}^6 \mu_{d,ij} \tilde{\tau}_{d,ij}^* \tilde{\tau}_{d,ij} \\ + \sum_{j=1}^6 \left(z_{2,ij} \tau_{M,ij} - |z_{2,ij}| \tau_{d,ij}^* + |z_{2,ij}| \tilde{\tau}_{d,ij}^* - z_{2,ij} \tilde{\tau}_{d,ij}^* \tanh\left(\frac{z_{2,ij} \tilde{\tau}_{d,ij}^*}{s}\right) \right) \quad (51)$$

Similar to Sect. 3.3, we have

$$\dot{V}_{2,i} \leq - \left(z_{1,i}^T K_{1,i} z_{1,i} + z_{2,i}^T K_{2,i} z_{2,i} - \frac{\|z_{2,i}\|^2}{2} + \sum_{j=1}^6 \frac{\mu_{d,ij} \|\tilde{\tau}_{d,ij}\|^2}{2} \right) \\ + \left(\frac{\|\varepsilon_{E,i}\|^2}{2} + \sum_{j=1}^6 \frac{\mu_{d,ij} \|\tau_{d,ij}^*\|^2}{2} + 1.671s \right) \\ \leq -\varsigma_2 V_{2,i} + \kappa_2 \quad (52)$$

where $\varsigma_2 = \min\{2\lambda(K_{1,i}), 2\lambda(K_{2,i}) - 1, \mu_{d,ij}\gamma_d\}$, $\kappa_2 = (\|\varepsilon_{E,i}\|^2/2 +$

$$\sum_{j=1}^6 \|\tilde{\tau}_{d,ij}\|^2/2 + 1.671s).$$

From (52), we obtain $V_{2,i} \leq V_{2,i}(0)e^{-\varsigma_2 t} + \mathcal{Q}_2$, which implies that the

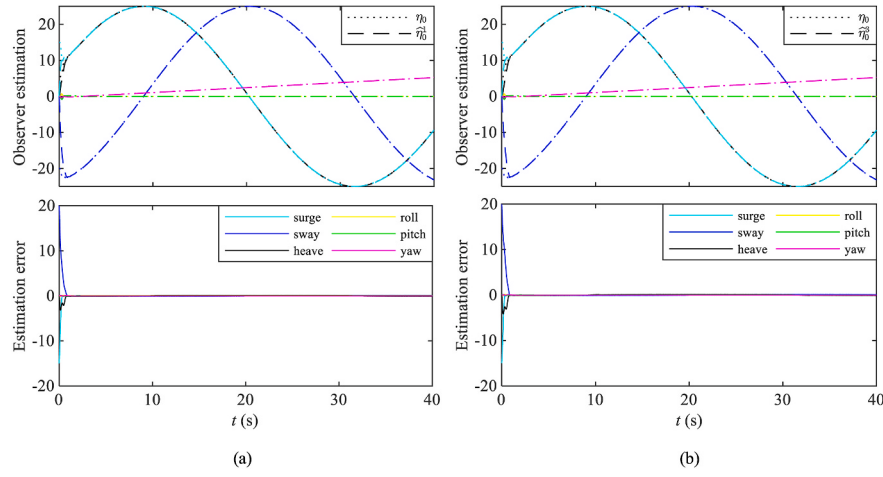


Fig. 3. Finite-time distributed observer state estimation. (a) Leader and Follower-1, (b) Leader and Follower-3.

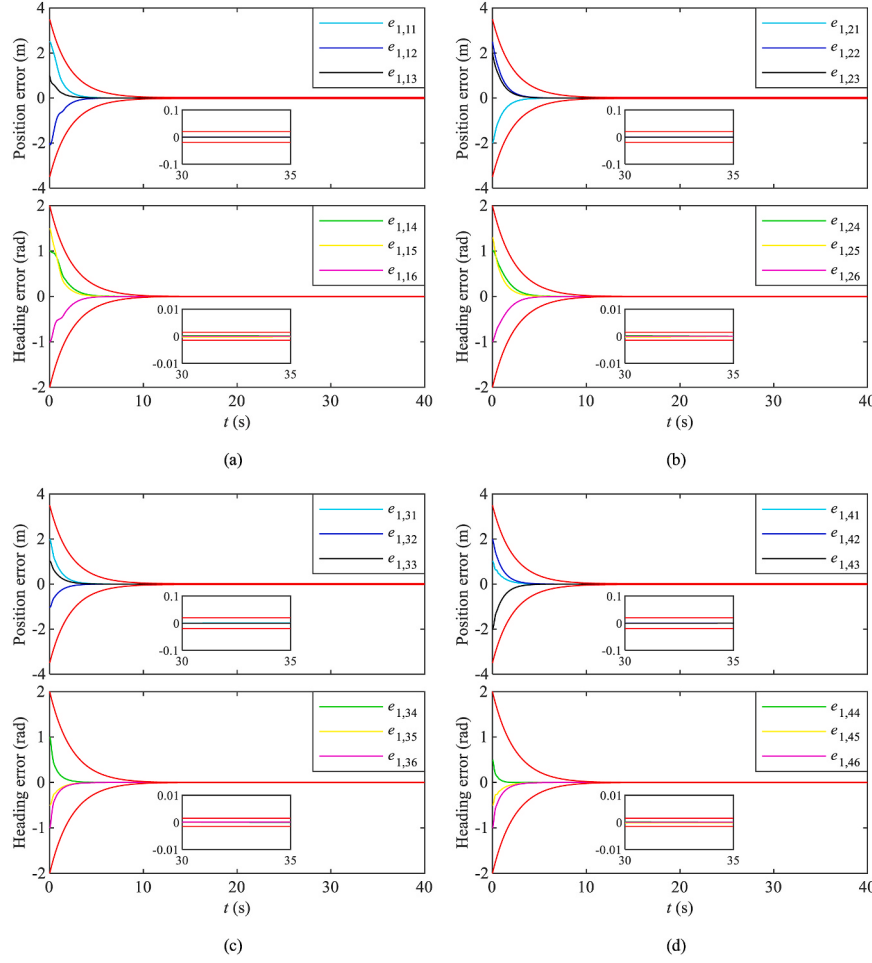


Fig. 4. Tracking errors under the control law (38). (a) Follower-1, (b) Follower-2, (c) Follower-3, (d) Follower-4.

following conclusions hold:

$$\|x_{1,i}\| \leq \sqrt{2\mathcal{Q}_2}, \|x_{2,i}\| \leq \sqrt{2\mathcal{Q}_2}, |\tilde{\tau}_{d,ij}| \leq \sqrt{2\mathcal{Q}_2\gamma_d} \quad (53)$$

where \$\mathcal{Q}_2\$ is an adjustable compact set.

Following the similar proof in Sect. 3.3, we conclude that (i) All state variables in the system are UUB. (ii) The trace error \$e_{1,i}\$ converges to an adjustable compact set in a finite time. ■

5. Simulation results

A group of simulation experiments on a multi-AUV system consisting of 5 AUVs are conducted to validate the proposed control laws. The dynamic information of AUVs is the same as that used in the literature (Wu et al., 2022). The desired formation configuration is described by \$\eta_1^* = [-1, 2, 0, 0, 0, 0]^T\$, \$\eta_2^* = [-1, -2, 0, 0, 0, 0]^T\$, \$\eta_3^* = [-5, 2, 0, 0, 0, 0]^T\$, and \$\eta_4^* = [-5, -2, 0, 0, 0, 0]^T\$. The unmodeled dynamic is given by \$\Delta(\eta_i)\$.

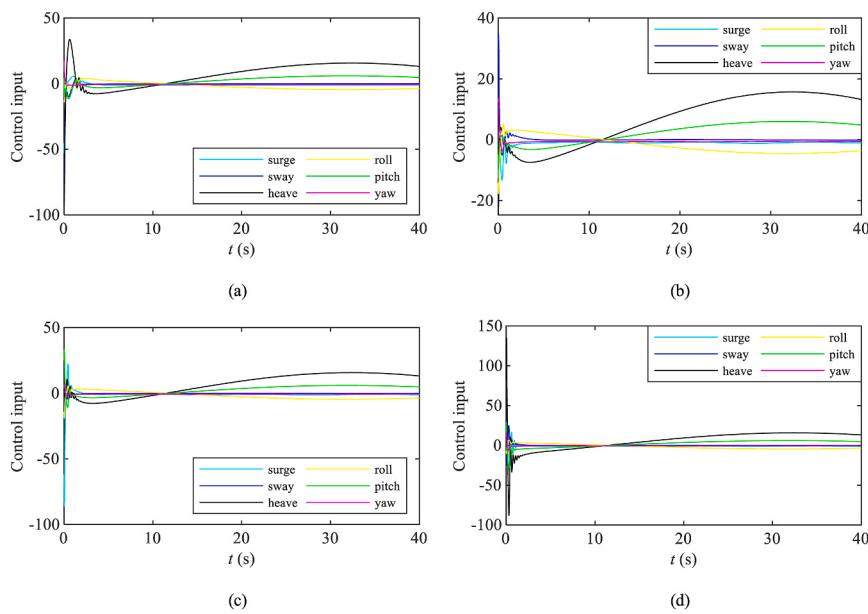


Fig. 5. Control input under the control law (38). (a) Follower-1, (b) Follower-2, (c) Follower-3, (d) Follower-4.

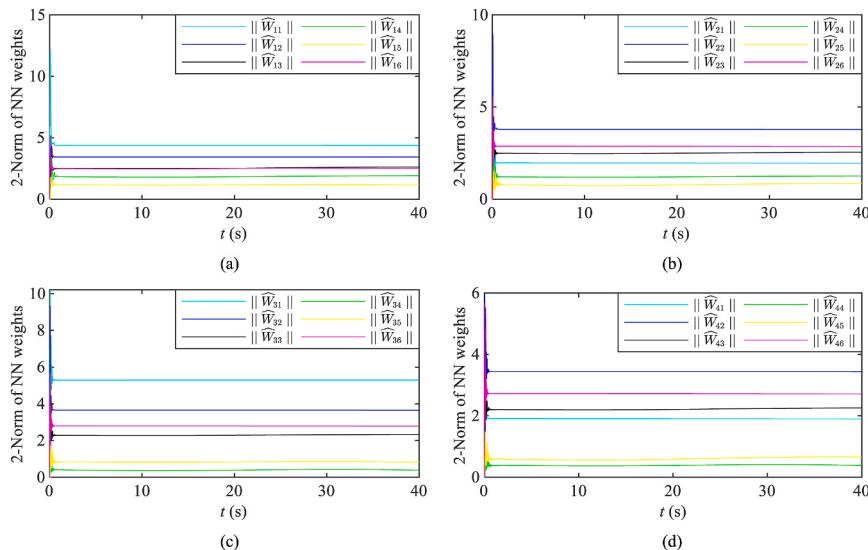


Fig. 6. 2-Norm of RBFNN weight estimation. (a) Follower-1, (b) Follower-2, (c) Follower-3, (d) Follower-4.

$v_i) = [\Delta_1, \dots, \Delta_6]^T$, where $\Delta_1 = \cos(u_i^2) + 1$, $\Delta_2 = 0.05v_i^2 + 1$, $\Delta_3 = \cos(0.1w_i^2) + 1$, $\Delta_4 = 1 - \cos(p_i^2)$, $\Delta_5 = 1 - \sin(q_i^2)$, and $\Delta_6 = 0.2 \sin(r_i^2)$. The external disturbance is designated as $\tau_d = [3 + 0.5 \cos(0.2t), 3 + 0.4 \sin(0.1t), 3 + 0.4 \cos(0.2t), 0, 0, 1 + 0.2 \sin(0.6t)]$. Fig. 1 depicts the communication topology. The parameterized path and the initial states of the AUVs are specified as shown in Table 1.

5.1. Simulation for controlling the velocity

In this part, an experiment is performed to verify the efficiency of the trajectory-following control law for the leader on velocity control. The parameters are given as $K_{1,0} = \text{diag}[0.5, 0.5, 0.5, 0.5, 0.5, 0.5]$, $K_{2,0} = \text{diag}[5, 5, 5, 5, 5, 5]$ and $k_p = 10$. The parameters in FTESO are designed as $m = 2$ and $\beta_1 = 0.8$. The parameterized path is given in [Table 1](#), where the desired path update rate $\dot{\sigma}_d$ is initially set to 1 and steps up to 2 after 15 s.

The results are presented in Fig. 2. Fig. 2 (a) indicates that the path

update rate $\dot{\sigma}$ converges rapidly to the desired value \mathcal{I} under the effect of the control law (12). Fig. 2 (b) demonstrates that the velocity of the leader can be designed independently using \mathcal{I} . Fig. 2 (c) shows the velocity error for the proposed parameterized path, which further validates the above conclusion.

5.2. Simulation for the formation control law using cooperative adaptive RBFNN

We first validate the effectiveness of the cooperative adaptive RBFNN-based control algorithm, with the control law for the leader given in Sect. 3.1 and the control law for followers given in Sect. 3.3. To approximate the dynamic uncertainties, we constructed RBFNNs $\widehat{W}_{ij}^T S_j(v_i)$, $i = 1 - 4, j = 1 - 6$, which contain 300 nodes whose centers are uniformly distributed in $[-10, 10]$ and whose widths are set to 2. The parameter values in the control law are designed as shown in Table 2.

The results are illustrated in Figs. 3–6. The position estimation

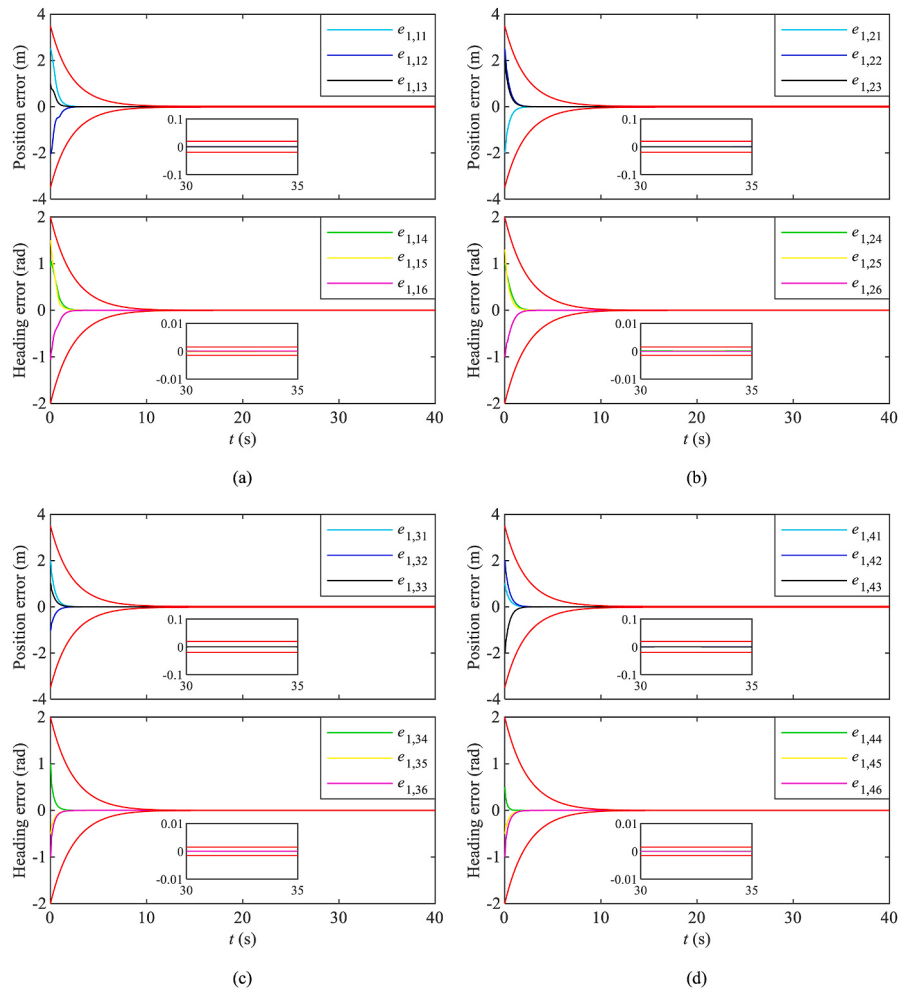


Fig. 7. Tracking errors under the empirically based formation control law (49). (a) Follower-1, (b) Follower-2, (c) Follower-3, (d) Follower-4.

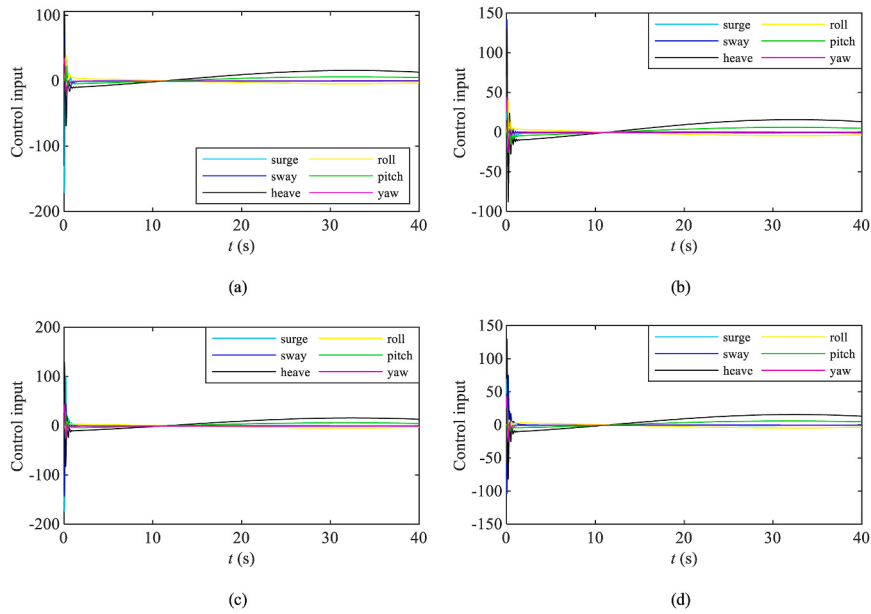


Fig. 8. Control input under the control law (49). (a) Follower-1, (b) Follower-2, (c) Follower-3, (d) Follower-4.

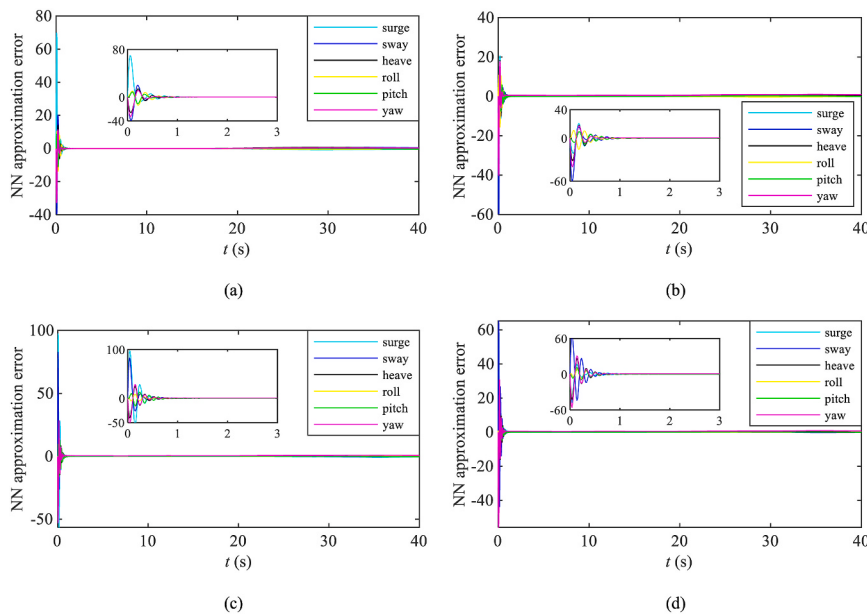


Fig. 9. RBFNN approximation errors using experience. (a) Follower-1, (b) Follower-2, (c) Follower-3, (d) Follower-4.

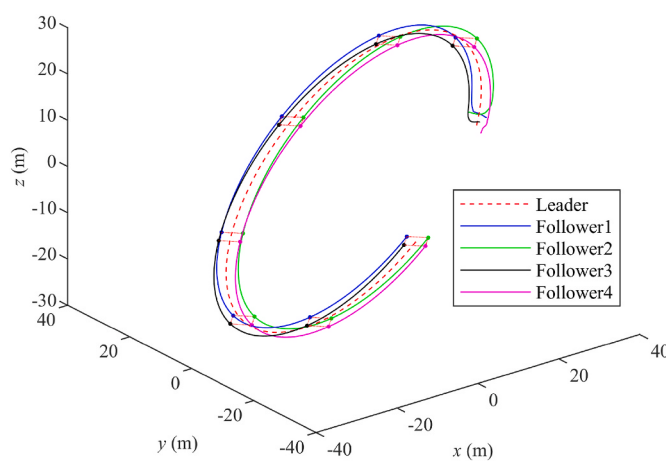


Fig. 10. Multi-AUVs formation control.

capability of the proposed FTDO (16) is illustrated in Fig. 3. Fig. 4 reveals that the tracking errors converge in finite time by using the trajectory-following control law (12) for the leader and the finite-time leader-following control law for followers (38). The control inputs using the control law (38) are shown in Fig. 5, which is bounded and practical. Fig. 6 demonstrates the convergence of RBFNN weights.

5.3. Simulation for formation control law using experience

We investigate the validity of the empirically based control law (49), whose tracking error is shown in Fig. 7. This result indicates that the empirically based control laws are equally capable of achieving accurate path tracking. The control inputs using the control law (49) are shown in Fig. 8, which demonstrates the feasibility for practical applications. The approximation errors for uncertainties are shown in Fig. 9, proving the effectiveness of the RBFNN using experience. Finally, the tracking performance is shown in Fig. 10, verifying that AUVs are capable of tracking the reference path while maintaining formation configuration.

6. Conclusion

This article addressed the formation control issue under communication constraints for multi-AUV systems with uncertainties and disturbances. The parameterized path was proposed to individually govern the velocity. The dynamic uncertainties were approximated and learnt cooperatively by the localized RBFNNs while tracking the period path, which means that experience was used in the control law instead of adaptive methods. The problem of communication constraints between the leader and followers was addressed by the finite-time distributed observer. The disturbances were effectively compensated by the specific method, and the finite-time control method was implemented to accelerate the learning process.

CRediT authorship contribution statement

Zilong Song: Conceptualization, Methodology, Writing – original draft, Writing – review & editing. **Zheyuan Wu:** Validation, Visualization, Software. **Haocai Huang:** Supervision, Project administration, Funding acquisition.

Declaration of competing interest

The authors declare that they have no known competing financial interests or personal relationships that could have appeared to influence the work reported in this paper.

Data availability

Data will be made available on request.

Acknowledgment

This work is supported by the project of the Donghai Laboratory (Grant number DH-2022ZY0004) and the National Key Research and Development Program of China (Grant number 2017YFC0306100).

References

- Bechlioulis, C.P., Karras, G.C., Heshmati-Alamdar, S., Kyriakopoulos, K.J., 2017. Trajectory tracking with prescribed performance for underactuated underwater

- vehicles under model uncertainties and external disturbances. *IEEE Trans. Control Syst. Technol.* 25 (2), 429–440.
- Cui, R.X., Chen, L.P., Yang, C.G., Chen, M., 2017a. Extended state observer-based integral sliding mode control for an underwater robot with unknown disturbances and uncertain nonlinearities. *IEEE Trans. Ind. Electron.* 64 (8), 6785–6795.
- Cui, R.X., Yang, C.G., Li, Y., Sharma, S., 2017b. Adaptive neural network control of AUVs with control input nonlinearities using reinforcement learning. *IEEE Trans. Syst., Man, Cybern., Syst.* 47 (6), 1019–1029.
- Dai, S.L., He, S.D., Ma, Y.F., Yuan, C.Z., 2022. Cooperative learning-based Formation Control of autonomous marine surface vessels with prescribed performance. *IEEE Trans. Syst., Man, Cybern., Syst.* 52 (4), 2565–2577.
- Fang, K., Fang, H., Zhang, J., Yao, J., Li, J., 2021. Neural adaptive output feedback tracking control of underactuated AUVs. *Ocean. Eng.* 234.
- Fei, Y., Shi, P., Lim, C.C., 2022. Neural-based formation control of uncertain multi-agent systems with actuator saturation. *Nonlinear Dynam.* 108 (4), 3693–3709.
- Fu, M., Wang, L., 2021. Adaptive finite-time event-triggered control of marine surface vehicles with prescribed performance and output constraints. *Ocean. Eng.* 238.
- Gao, Z.Y., Guo, G., 2020. Fixed-time sliding mode formation control of AUVs based on a disturbance observer. *IEEE/CAA J. Autom. Sinica* 7 (2), 539–545.
- Huang, B., Zhou, B., Zhang, S., Zhu, C., 2021. Adaptive prescribed performance tracking control for underactuated autonomous underwater vehicles with input quantization. *Ocean. Eng.* 221.
- Kong, S.H., Sun, J.L., Qiu, C.L., Wu, Z.X., Yu, J.Z., 2021. Extended state observer-based controller with model predictive governor for 3-D trajectory tracking of underactuated underwater vehicles. *IEEE Trans. Ind. Inf.* 17 (9), 6114–6124.
- Lin, Z., Wang, H.D., Karkoub, M., Shah, U.H., Li, M., 2021. Prescribed performance based sliding mode path-following control of UVMS with flexible joints using extended state observer based sliding mode disturbance observer. *Ocean. Eng.* 240.
- Liu, H., Wang, Y.H., Lewis, F.L., 2021a. Robust distributed formation controller design for a group of unmanned underwater vehicles. *IEEE Trans. Syst., Man, Cybern., Syst.* 51 (2), 1215–1223.
- Liu, J., Wang, C., Cai, X., 2021b. Adaptive neural network finite-time tracking control for a class of high-order nonlinear multi-agent systems with powers of positive odd rational numbers and prescribed performance. *Neurocomputing* 419, 157–167.
- Liu, L., Wang, D., Peng, Z.H., 2019. State recovery and disturbance estimation of unmanned surface vehicles based on nonlinear extended state observers. *Ocean. Eng.* 171, 625–632.
- Liu, S.Y., Liu, Y.C., Wang, N., 2017. Nonlinear disturbance observer-based backstepping finite-time sliding mode tracking control of underwater vehicles with system uncertainties and external disturbances. *Nonlinear Dynam.* 88 (1), 465–476.
- Ly, J.Q., Wang, Y., Tang, C., Wang, S., Xu, W.X., Wang, R., Tan, M., 2022. Disturbance rejection control for underwater free-floating manipulation. *IEEE ASME Trans. Mechatron.* 27 (5), 3742–3750.
- Peng, Z.H., Wang, D., Li, T.S., Han, M., 2020. Output-Feedback cooperative formation maneuvering of autonomous surface vehicles with connectivity preservation and collision avoidance. *IEEE Trans. Cybern.* 50 (6), 2527–2535.
- Peng, Z.H., Wang, J.S., Wang, J., 2019. Constrained control of autonomous underwater vehicles based on command optimization and disturbance estimation. *IEEE Trans. Ind. Electron.* 66 (5), 3627–3635.
- Qiao, L., Zhang, W.D., 2020. Trajectory tracking control of AUVs via adaptive fast nonsingular integral terminal sliding mode control. *IEEE Trans. Ind. Inf.* 16 (2), 1248–1258.
- Rong, S., Wang, H., Li, H., Sun, W., Gu, Q., Lei, J., 2022. Performance-guaranteed fractional-order sliding mode control for underactuated autonomous underwater vehicle trajectory tracking with a disturbance observer. *Ocean. Eng.* 263.
- Shen, C., Shi, Y., Buckingham, B., 2018. Trajectory tracking control of an autonomous underwater vehicle using lyapunov-based model predictive control. *IEEE Trans. Ind. Electron.* 65 (7), 5796–5805.
- Sun, K.K., Qiu, J.B., Karimi, H.R., Fu, Y.L., 2021. Event-Triggered robust fuzzy adaptive finite-time control of nonlinear systems with prescribed performance. *IEEE Trans. Fuzzy Syst.* 29 (6), 1460–1471.
- Wang, C., Hill, D.J., 2006. Learning from neural control. *IEEE Trans. Neural Network.* 17 (1), 130–146.
- Wang, M., Wang, C., 2015. Learning from adaptive neural dynamic surface control of strict-feedback systems. *IEEE Transact. Neural Networks Learn. Syst.* 26 (6), 1247–1259.
- Wei, H.L., Shen, C., Shi, Y., 2021. Distributed lyapunov-based model predictive formation tracking control for autonomous underwater vehicles subject to disturbances. *IEEE Trans. Syst., Man, Cybern., Syst.* 51 (8), 5198–5208.
- Wu, X.R., Huang, Y.Y., 2022. Adaptive fractional-order non-singular terminal sliding mode control based on fuzzy wavelet neural networks for omnidirectional mobile robot manipulator. *ISA Trans.* 121, 258–267.
- Wu, Z.Y., Wang, Q., Huang, H.C., 2022. Adaptive neural networks trajectory tracking control for autonomous underwater helicopters with prescribed performance. *Ocean. Eng.* 264.
- Xu, B., Wang, Z., Shen, H., 2022a. Distributed predictive formation control for autonomous underwater vehicles under dynamic switching topology. *Ocean. Eng.* 262.
- Xu, J., Cui, Y., Xing, W., Huang, F., Du, X., Yan, Z., Wu, D., 2022b. Distributed active disturbance rejection formation containment control for multiple autonomous underwater vehicles with prescribed performance. *Ocean. Eng.* 259.
- Yuan, C.Z., He, H.B., Wang, C., 2019. Cooperative deterministic learning-based Formation Control for a group of nonlinear uncertain mechanical systems. *IEEE Trans. Ind. Inf.* 15 (1), 319–333.
- Yuan, C.Z., Licht, S., He, H.B., 2018. Formation learning control of multiple autonomous underwater vehicles with heterogeneous nonlinear uncertain dynamics. *IEEE Trans. Cybern.* 48 (10), 2920–2934.
- Zhou, B., Su, Y., Huang, B., Wang, W., Zhang, E., 2022. Trajectory tracking control for autonomous underwater vehicles under quantized state feedback and ocean disturbances. *Ocean. Eng.* 256.
- Zong, G.D., Sun, H.B., Nguang, S.K., 2021. Decentralized adaptive neuro-output feedback saturated control for INS and its application to AUV. *IEEE Transact. Neural Networks Learn. Syst.* 32 (12), 5492–5501.